

Timing Inaccessibility and the Projection Bound: Resolving Maxwell’s Demon for Continuous Biological Substrates

Version 2.0

Ian Todd

Sydney Medical School

University of Sydney

Sydney, NSW, Australia

itod2305@uni.sydney.edu.au

December 2025

Abstract

Maxwell’s demon was resolved by Landauer and Bennett: the demon must erase information to reuse its memory, paying $\geq k_B T \ln 2$ per bit. But this resolution assumed discrete memory states. We extend the resolution to continuous biological substrates, showing that the thermodynamic advantage of living systems arises from *timing inaccessibility*: irreversibly registering fine temporal order at resolution Δt requires exporting $\geq k_B T \ln 2$ per stabilized order bit; when the relevant couplings are sub-Landauer, extracting such records without dominating the dynamics requires measurement resources that overwhelm the coupling energies (back-action). Consequently, exponentially many micro-trajectories map to the same observable outcome (*path degeneracy*). Continuous

high-dimensional substrates exploit this by integrating sub-Landauer couplings during evolution and paying only at *projection* (dimensional collapse to a low-dimensional output).

We derive a **Projection Bound** for quasistatic projection at effective temperature T_{eff} :

$$E_{\text{collapse}} \geq k_{\text{B}} T_{\text{eff}} \left(\ln \frac{N_{\varepsilon, \text{pre}}}{N_{\varepsilon, \text{post}}} - \text{KL}(p^{\text{pre}} \| U_{\text{pre}}) + \text{KL}(p^{\text{post}} \| U_{\text{post}}) \right) \quad (0.1)$$

which reduces under typical-set conditions to $E_{\text{collapse}} \geq k_{\text{B}} T_{\text{eff}} \ln(N_{\varepsilon, \text{pre}}/N_{\varepsilon, \text{post}})$. Combined with a **Temporal Registration Bound** (order over M bins needs $\log_2 M!$ bits), we quantify the gap: digital tracking requires *thermodynamic registration* of $\log_2 G \sim D \log k$ bits (linear in D but with $\sim 10^4\text{--}10^6 \times$ practical overhead), whereas continuous substrates defer cost to projection, paying $\sim D \ln(L/\varepsilon)$ only at collapse.

Version 2.0 extends the analysis with three new arguments: (1) *Framework dependence of timing*—the measurement framework itself determines what counts as “simultaneous” versus “sequential,” making temporal structure framework-relative in the same sense that falsifiability is framework-relative [4]. (2) *The “when” is created, not revealed*—temporal order does not pre-exist measurement but emerges at projection, with conceptual implications for causality and agency (explored speculatively). (3) *AI substrate constraints*—digital substrates cannot access the sub-Landauer integration regime regardless of scale, suggesting mechanism-level limits on what digital AI can achieve (though behavioral approximation may remain possible).

For biologically plausible parameters, we estimate degeneracies of $10^{42}\text{--}10^{94}$ (protein folding) and $10^{50}\text{--}10^{100}$ (neural dynamics) as upper bounds under independence assumptions. The framework reconciles stochastic resonance (amplitude detection) with order inaccessibility, and clarifies why analog/neuromorphic systems gain efficiency by deferring projection.

Keywords: Maxwell’s demon, timing inaccessibility, path degeneracy, Landauer principle, dimensional collapse, framework dependence, AI capability limits

Significance

What's new? A geometric thermodynamic bound showing that continuous high-dimensional substrates pay once at projection, not per micro-decision.

Why it matters? It explains biology's energy efficiency without violating the second law: sense weakly (sub-Landauer), integrate across many modes, and collapse late.

Numbers: Order-of-magnitude path degeneracies of 10^{42} – 10^{94} (proteins) and 10^{50} – 10^{100} (neural) arise for typical (D_{eff} , τ_c , Δt) (see Appendix A for parameter sensitivity).

Testable: (i) $\tau_c \uparrow \rightarrow$ accuracy \uparrow ; (ii) D_{eff} shifts across frequency-specific constraint channels with task; (iii) decision-time heat $\approx k_B T_{\text{eff}} \ln(N_{\text{pre}}/N_{\text{post}})$ at attojoule scale (~ 0.03 – 1 aJ). For example, ordering $M=10$ bins requires $\log_2(10!) \cdot k_B T \ln 2 \approx 6.3 \times 10^{-20}$ J (0.063 aJ) at 300 K—this is the *theoretical minimum* (the bound); estimated *biological* collapse costs for neural decisions with $D_{\text{eff}} \sim 50$ – 200 are $\sim 10^{-19}$ – 10^{-18} J.

1 Introduction

High-dimensional systems exist as physical and mathematical objects. When you need to compute what such a system does, you face an implementation choice: simulate it on a low-dimensional digital substrate (bit strings), or instantiate it physically as a high-dimensional system. This paper quantifies the thermodynamic efficiency gap between these approaches.

1.1 The Biological Maxwell's Demon

Living systems operate in a Maxwell–demon–like mode. They:

- create local order (cells, organisms, structured neural activity) from stochastic environments,
- extract work from thermal and chemical gradients,
- maintain far-from-equilibrium organization over decades, and

- process information to guide adaptive responses.

The energetic puzzle is stark: a human brain performs sophisticated computations at ~ 20 W, whereas comparable digital systems require orders of magnitude more power [35, 36]. If biological systems *acquired and recorded* information as discrete bits, Landauer’s principle would demand a dissipation of at least $k_B T \ln 2$ per bit. Yet measured neural energetics are far below what such pervasive bit-level bookkeeping would imply.

We consider three possibilities:

1. **Physics violation** — biology evades the second law (ruled out empirically).
2. **Hidden costs** — the energy is dissipated elsewhere, unmeasured (possible but unsimonious).
3. **Different accounting** — continuous high-dimensional substrates store and use information as *structural correlations*, not as stabilized bits; the thermodynamic payment appears only at *projection* (this paper’s thesis).

We demonstrate (iii): biological systems maintain information as correlations in high- D coherence fields and defer irreversible registration. The cost is paid when those correlations are collapsed to discrete actions — the dimensional projection. Between acquisition and projection, information exists physically (in coupled dynamics) without bit erasure, enabling apparent sub-Landauer operation locally while preserving global thermodynamic consistency.

Central mechanism (preview). Below the Landauer threshold ($k_B T \ln 2 \approx 2.87 \times 10^{-21}$ J at 300 K), *temporal order cannot be irreversibly registered* without dissipating at least $k_B T \ln 2$ per binary timing decision. This *timing inaccessibility* creates exponential path degeneracy: many micro-trajectories map to the same observable outcome. Digital systems that track order pay per recorded bit; continuous high- D substrates integrate weak, sub-Landauer couplings and pay once at projection. See Lemma 2.1 and Eq. 1.2 for the Temporal Registration Bound and the Projection Bound.

Critical distinction—the two-stage model: Throughout this paper, we distinguish two stages of information processing:

1. **Stage 1: Reversible coupling/correlation formation.** The system couples to its environment, creating mutual information through physical correlation. This can occur at sub-Landauer energies ($E_{\text{link}} \ll k_B T \ln 2$ per coupling) and leaves no persistent, queryable record. Information exists in the joint state of system and environment, not as “written bits.” This stage is thermodynamically cheap (in principle, free for ideal reversible processes).
2. **Stage 2: Stabilization/registration (projection).** The correlation is collapsed to a persistent, reusable record—a measurement outcome, a decision, a discrete state. This is logically irreversible (cannot be undone without external information) and incurs the Landauer cost: $\geq k_B T \ln 2$ per bit stabilized.

Biological systems exploit this distinction: they perform extensive Stage 1 processing (sensing, integrating, correlating across many channels) while deferring Stage 2 (projection/collapse) to the final output. Digital systems, by contrast, perform Stage 2 at the input boundary—every value entering the digital domain must first be stabilized as bits. This architectural difference explains the efficiency gap.

1.2 The Demon’s Lineage: From Maxwell to Biology

The Maxwell’s demon problem has a precise intellectual history that this paper extends:

Maxwell (1867): Proposed a “finite being” that could sort fast and slow molecules between chambers, apparently creating temperature gradients (and extracting work) without doing work itself—violating the second law [28].

Szilard (1929): Formalized the demon as a thermodynamic engine. In Szilard’s single-molecule engine, the demon (i) measures which half of a box contains a molecule, (ii) inserts

a partition, and (iii) extracts $k_B T \ln 2$ of work via isothermal expansion. Szilard showed that the demon must acquire information to operate, connecting information to thermodynamics [29].

Landauer (1961): Identified the cost: not measurement, but *erasure*. Any logically irreversible operation (including resetting memory to reuse it) dissipates at least $k_B T \ln 2$ per bit [1]. The demon can measure for free (in principle) but must eventually erase its memory, paying the thermodynamic cost.

Bennett (1973, 1982): Completed the resolution. The demon’s memory is finite; to continue operating, it must erase old measurements. This erasure cost exactly compensates the work extracted. The second law is saved [27].

This paper (2025): Extends the resolution to continuous substrates. The Landauer-Bennett resolution assumed discrete memory states (bits). Biological systems operate with continuous, high-dimensional dynamics where “memory” is structural correlation, not written bits. We show that continuous substrates defer the Landauer cost via path degeneracy: exponentially many micro-trajectories map to the same outcome, and the thermodynamic payment occurs only at *projection* (dimensional collapse). The biological demon doesn’t write and erase—it correlates and collapses.

Scope note. “Maxwell’s demon” here is not merely metaphor—it is the literal extension of the Szilard-Landauer-Bennett framework to continuous, classical, room-temperature substrates. No violation of the second law is implied; we identify where the thermodynamic cost appears.

Three levels of claims. This paper makes claims at three distinct levels, which readers should evaluate separately:

1. **Thermodynamic/engineering claim** (Sections 2–5): Irreversibly stabilizing temporal-order information requires $\geq k_B T \ln 2$ per bit. This is the most defensible claim and follows directly from Landauer’s principle.
2. **Operational-access claim** (Sections 2–5): Below some energy/precision regime, tem-

poral order is not practically accessible without unacceptable disturbance or back-action. This is plausible but depends on modeling assumptions about measurement.

3. **Interpretive claim** (Sections 7–8): The “when” does not exist until projection; temporal order is created, not revealed. This is philosophically interesting but should be understood as an *interpretation* layered atop claims (1–2), not a direct consequence of thermodynamics. Skeptical readers can accept the bounds without endorsing this metaphysics.

Main Results

Temporal Registration Bound (TRB): Irreversibly recording the total order of M temporal bins requires $\log_2(M!)$ bits (by Stirling: $\log_2(M!) \geq M \log_2 M - M \log_2 e$ for large M), hence:

$$E_{\min}^{\text{time}} \geq k_B T \ln 2 \cdot \log_2(M!) \quad (1.1)$$

Projection Bound (PB): Quasistatic projection from $N_{\varepsilon,\text{pre}}$ to $N_{\varepsilon,\text{post}}$ distinguishable states dissipates:

$$E_{\text{collapse}} \geq k_B T_{\text{eff}} \ln(N_{\varepsilon}(D_{\text{eff}})/N_{\varepsilon}(D')) \quad (1.2)$$

under typical-set approximation (equiprobable cells).

Path Degeneracy Scaling: With coherence time τ_c and temporal resolution Δt :

$$\Omega(\Delta t) \sim \exp\left[\frac{D_{\text{eff}}(\Delta t)}{\kappa} \ln \frac{\tau_c}{\Delta t}\right] \quad (1.3)$$

where $\kappa \geq 1$ accounts for correlations.

1.3 Efficiency Gap: Where the Energy Goes

Digital algorithm tracking the path:

- To uniquely index among G options: $\log_2 G$ bits required
- Protein folding: $\log_2(10^{48-100}) \approx 160-332$ bits

- Energy dissipated during tracking: $E_{\text{digital}} \gtrsim (160-332)k_B T \ln 2 \approx 4.6 \times 10^{-19}-9.5 \times 10^{-19} \text{ J}$ (ideal Landauer floor; practical CMOS is $10^4-10^6 \times$ higher, while fully reversible logic can approach the floor only with severe speed and noise-tolerance tradeoffs [27, 36])
- This applies even if history is later discarded—the cost was paid during recording

Continuous substrate (deferred projection):

- System samples all $\sim 10^{48}-10^{100}$ conformations via thermal fluctuations
- No irreversible records made during exploration
- Pay only at projection: $E_{\text{cont}} \geq k_B T_{\text{eff}} \ln 2$ for binary collapse ("native" vs. "mis-folded")

Efficiency gain: $\sim 160-330 \times$ at theoretical Landauer limit. Contemporary CMOS operates at $\sim 10^4-10^6 \times$ Landauer limit, raising practical gap to $\sim 10^5-10^8 \times$ [35, 36]. While adiabatic reversible computing could theoretically narrow this gap [27, 36], practical implementations face severe speed and noise-tolerance tradeoffs. Digital architectures pay per recorded bit; continuous substrates defer recording and pay at projection. Analog/neuromorphic systems likewise gain efficiency by deferring discretization to the projection boundary.

Note on scaling: The *registration cost* to identify/record one trajectory class is $\sim \log_2 G$, which scales linearly with D when $G \sim k^D$. However, *explicit state evolution*—simulating fine-grained dynamics or exploring the full trajectory space—can require exponential compute/time in D . Throughout this paper, we focus primarily on the thermodynamic cost of irreversible registration, which is the tighter bound for biological substrates.

1.4 Notation and Conventions

Connection to framework formalism. The companion paper [4] (and its v2.0 extension) defines a *framework* $\mathcal{F} = (M, R, D)$ as a triple of maps: measurement $M : X \rightarrow Y$, represen-

Table 1: Key symbols and definitions

Symbol	Definition
$k_B T \ln 2$	Landauer bound per bit ($\approx 2.87 \times 10^{-21}$ J at 300 K)
T	Bath temperature (K); used in TRB
$T_{\text{eff}}(\omega)$	Effective temperature at frequency ω via FDT (K); defined operationally at collapse mode; used in PB
D_{eff}	Effective dimensionality, $(\sum_i \lambda_i)^2 / \sum_i \lambda_i^2$
D'	Post-collapse effective dimensionality (output manifold dimension)
N_ε	Covering number: count of ε -balls covering manifold
G, Ω	Path degeneracy (number of micro-trajectories per macro-outcome); used synonymously
τ_c	Coherence time, $\int_0^\infty \langle r(t)r(0) \rangle dt$ (s)
Δt	Temporal resolution (s)
κ	Correlation factor ≥ 1 (reduces degeneracy from independence)
ε	Coarse-graining resolution
L	System size (same units as ε ; L/ε is dimensionless)
ξ	Correlation (coherence) length in capacity expressions

Conventions:

Natural logarithms (nats) unless stated; $\log_2 x = \ln x / \ln 2 \approx 1.443 \ln x$

Energy: $k_B T$ per nat or $k_B T \ln 2$ per bit

Typical set: high-probability subset under source measure (Cover & Thomas)

tation $R : Y \rightarrow Z$, and decision $D : Z \rightarrow \{0, 1\}$. Each framework induces a partition on the state space X , and *projection loss* $\mathcal{L}(\mathcal{F}) := H(X) - I(X; Z)$ quantifies how much information about X is destroyed by the framework choice. Here, temporal resolution Δt is a component of M —the choice of Δt determines what counts as “simultaneous” versus “sequential” and thereby determines which causal relationships are visible. Framework dependence of timing (§7) is a special case of the general framework dependence of falsifiability.

1.5 Roadmap

Section 2 formalizes timing inaccessibility. Section 3 derives the Projection Bound. Section 4 quantifies path degeneracy. Section 5 gives a continuous (Kuramoto) example. Section 6 relates to prior work and discusses implications including camera-engine duality. **Version 2.0 additions:** Section 7 establishes framework dependence of timing. Section 8 argues

that temporal order is created at projection, not revealed. Section 9 derives implications for AI capability limits. Appendix A provides parameter sensitivity analysis for degeneracy estimates. Appendix B describes biological implementations across scales. Appendix C provides methods for estimating D_{eff} and κ from data.

2 Timing Inaccessibility: The Physical Mechanism

What would falsify timing inaccessibility? A demonstration of stable temporal-order records formed at sub-Landauer energy cost *without* pushing dissipation elsewhere (hidden reservoirs, pre-amplification) or causing back-action that disrupts the system being tracked. In other words: show a persistent, queryable record of fine temporal ordering where the total energy cost (including all auxiliary systems) is less than $k_B T \ln 2$ per stabilized order bit. Absent such a demonstration, the TRB stands.

2.1 Why Temporal Order Costs More Than Amplitude

Following Todd (2025) [4], for reliable bit-level readout under thermal noise at temperature T with irreversible stabilization, measurement at energy E_{meas} extracts information bounded by:

$$I_{\max} \lesssim \frac{E_{\text{meas}}}{k_B T \ln 2} \quad (2.1)$$

This bound follows from the AWGN limit where reliable bit recovery (error probability bounded away from 1/2) demands $E_b/N_0 \geq \ln 2$ [40, 33]. **Detection capacity (AWGN, $E_b/N_0 \geq \ln 2$) is separate from recording/erasure cost (Landauer, $\geq k_B T \ln 2$ per bit).** The former bounds channel capacity (cf. Verdú's $E_b/N_0 \geq \ln 2$); the latter applies when information is irreversibly stabilized as memory (Landauer's $k_B T \ln 2$).

For a fixed measurement window with finite-time, finite-bandwidth channels and error probability bounded away from 1/2, when $E_{\text{meas}} \ll k_B T \ln 2$, you cannot extract even one bit reliably. This means *irreversible registration of temporal order* fails—the system may still

sense and integrate timing information, but cannot stabilize it as persistent memory.

Lemma 2.1 (Temporal Registration Bound). *To irreversibly register the temporal order of M bins requires at least $H \geq \log_2(M!)$ bits. By Landauer’s principle, the minimal dissipated energy is:*

$$E_{\min}^{\text{time}} \geq k_B T \ln 2 \cdot \log_2(M!) \quad (2.2)$$

For partial order distinguishing equivalence classes of sizes m_j :

$$E_{\min}^{\text{time}} \geq k_B T \ln 2 \cdot \log_2 \left(\frac{M!}{\prod_j m_j!} \right) \quad (2.3)$$

At sub-Landauer energies where $E_{\text{meas}} \ll k_B T \ln 2$, the number of binary timing decisions that can be irreversibly registered approaches zero.

Proof. See Appendix A. □

Scope conditions: TRB is a worst-case bound for recording a *full permutation-class history* at resolution Δt . If the task only requires partial order or coarse temporal features (e.g., “which of 3 phases” rather than full ordering of $M = 10$ bins), replace $M!$ by the size of the relevant equivalence-class space (Eq. 2.3). For example, distinguishing only K equivalence classes among M bins requires $\log_2 \binom{M}{K}$ bits, not $\log_2(M!)$ bits.

Clarification: A reversible comparator that leaves no persistent record can, in principle, avoid dissipation. The energetic bound applies when the order is *stabilized as memory* (logically irreversible). This is precisely the Landauer-Bennett point: the cost is in *erasure/stabilization*, not measurement per se.

Measurement model (why “timing inaccessibility” is physical, not just formal):

A likely objection is that Landauer’s principle concerns logically irreversible operations (erasure/reset), not the energy scale of underlying events—in principle, one can always spend external energy to measure something tiny. The subtlety is this: if each microscopic interaction has energy $\ll k_B T \ln 2$, then any attempt to obtain a *reusable, stable, queryable record* of

detailed temporal ordering requires measurement apparatus with coupling strength and/or energy that (i) *swamps the signal* relative to thermal noise, and (ii) *causes non-negligible back-action* on the system being tracked. You cannot simultaneously keep the system in its native weak-coupling regime *and* extract a full micro-order history. The energetic cost is dissipated in the measurement apparatus (not the system), but that cost is unavoidable for irreversible registration. This is why “timing inaccessibility” is an operational constraint, not merely an accounting choice.

Concrete example: At $T = 300\text{ K}$, ordering $M = 10$ bins minimally dissipates $\log_2(10!)$.
 $k_B T \ln 2 \approx 21.8 \times 2.87 \times 10^{-21} \text{ J} \approx 6.3 \times 10^{-20} \text{ J}$.

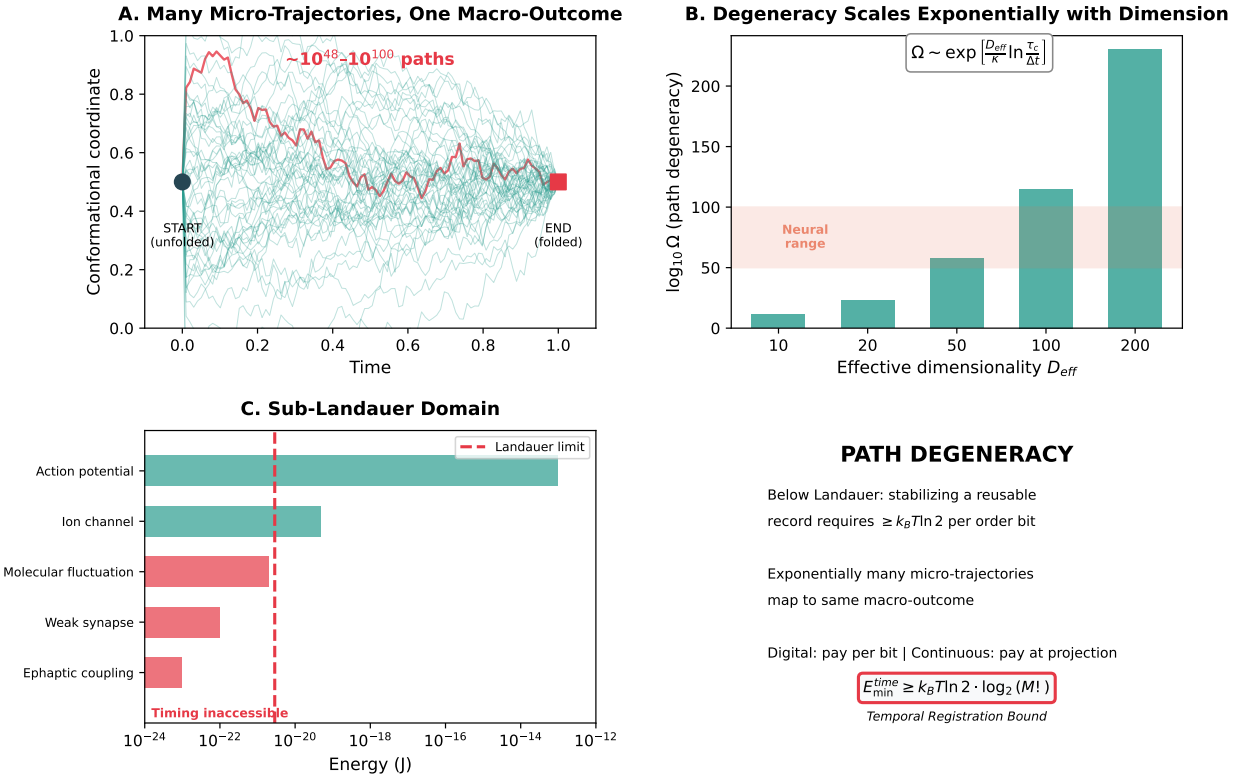


Figure 1: Path degeneracy and the sub-Landauer domain. (A) Many micro-trajectories map to the same macro-outcome (e.g., “protein folded”). (B) Degeneracy scales exponentially with effective dimensionality. (C) The sub-Landauer regime: when coupling energies are $\ll k_B T \ln 2$ ($\approx 2.87 \times 10^{-21} \text{ J}$ at 300 K), irreversibly stabilizing a reusable record of fine temporal order requires measurement resources that dominate the coupling energies (back-action), making micro-order operationally inaccessible without paying $\geq k_B T \ln 2$ per stabilized order bit. (D) Key insight: path degeneracy is not a bug but a feature enabling weak-signal integration.

2.2 Stochastic Resonance: Why It Detects Amplitude But Not Order

Natural objection: If stochastic resonance enables detection of sub-Landauer signals through population integration [5, 6], doesn't this eliminate path degeneracy?

Answer: No. Stochastic resonance provides:

- Amplitude/presence detection ($\text{SNR} \sim \sqrt{N}$ scaling)
- Population-level integration across N coupled units
- Knowledge that coordination occurred

It *cannot* provide:

- Timing of individual events (which fluctuation occurred when)
- Temporal ordering (did event A precede B?)
- Which specific coordination pattern was realized

For $M = 10$ temporal bins, distinguishing all orderings requires $\log_2(10!) \approx 21.8$ bits, costing $\geq 6.3 \times 10^{-20}$ J. If individual signal energies are $E \sim 10^{-23}$ J (sub-Landauer), measurement energy exceeds signal energy by $6000\times$. Population integration can detect *that* 10 events occurred, but not *when* or in what order.

Key distinction: Stochastic resonance improves detection of a *statistic* (coordination, amplitude) across a population, not the micro-order history of individual events. SR detects “how many” and “how strong,” not “which one when.”

2.3 High Dimensionality: The Key to Sub-Landauer Sensing

The puzzle: If individual events are sub-Landauer, how does the system sense anything?

The solution: The physical substrate is formally infinite-dimensional with power-law mode distribution. At any finite energy/temporal resolution, D_{eff} is finite and grows with

precision. At energy threshold E_{thresh} , a finite number of modes $D_{\text{eff}}(E_{\text{thresh}})$ carry energy $\geq E_{\text{thresh}}$.

With D_{eff} accessible modes, a signal of energy $E_{\text{signal}} \ll k_B T \ln 2$ per component can still be detected if integrated:

$$E_{\text{total}} \approx N_{\text{eff}} E_{\text{signal}}, \quad N_{\text{eff}} \propto D_{\text{eff}} \times \ln \frac{\tau_c}{\Delta t} \quad (2.4)$$

Even if $E_{\text{signal}} \ll k_B T \ln 2$ per channel, $E_{\text{total}} \gtrsim k_B T \ln 2$ achieves detectability.

Example: Neural population with $D_{\text{eff}} \sim 1000$ accessible modes can detect signals where each mode receives only $E_{\text{signal}} \sim 10^{-3} k_B T \ln 2$ because population integration yields effective energy $E_{\text{total}} \sim 1000 \times 10^{-3} k_B T \ln 2 = k_B T \ln 2$, meeting the detection threshold.

Ephaptic coupling: Extracellular fields $\sim 0.1\text{--}1$ mV/mm over neuronal membrane ($C_m \sim 1 \mu\text{F}/\text{cm}^2$) yield work $\sim 10^{-23}\text{--}10^{-22}$ J per neuron ($\approx 3 \times 10^{-3}\text{--}3 \times 10^{-2}$ times $k_B T \ln 2$) (see [39] for field strengths and scaling).

2.4 Why Digital Systems Cannot Do This

Fundamental architectural difference:

Digital systems:

- Binary bit requires $\geq k_B T \ln 2$ to be irreversibly registered
- Must receive supra-Landauer signals per input bit
- Cannot integrate sub-Landauer signals across channels without first amplifying each channel above threshold (costs energy)
- Must discretize each input above Landauer threshold before processing

Continuous high-D systems:

- Can couple weakly (sub-Landauer per link) to many sources

- Integrate via population dynamics
- Collapse only at output
- Pay for dimensional reduction, not per-interaction bit registration

The degeneracy is not a bug—it's what enables weak coupling to be computationally useful. Path degeneracy and sensing capability are coupled: exponentially many microstates allow sensitivity to distributed sub-Landauer perturbations.

3 The Projection Bound

3.1 What Are We Paying For?

When forcing a high-dimensional system to produce a low-dimensional output, you must dissipate heat. The cost has three components:

- 1. Geometric squashing** ($\ln N_{\varepsilon,\text{pre}}/N_{\varepsilon,\text{post}}$): How many configurations are you destroying? For continuous manifolds, $N_\varepsilon \sim (L/\varepsilon)^{D_{\text{eff}}}$ where L/ε is dimensionless.
- 2. Pre-collapse non-uniformity** ($-\text{KL}(p^{\text{pre}}\|U_{\text{pre}})$): Were you using all states uniformly? If the system had a heavy-tailed distribution, you were effectively more constrained than geometry suggests. This *lowers* the bound (you've already "paid" some entropy reduction).
- 3. Post-collapse specificity** ($+\text{KL}(p^{\text{post}}\|U_{\text{post}})$): How peaked is your final state? This *increases* the bound—you're creating more order.

Typical-set approximation: For high-dimensional systems with many weakly-interacting modes, equipartition and maximum entropy drive toward near-uniform occupancy. When both pre- and post-collapse distributions are approximately uniform, KL terms vanish and you get the clean geometric bound.

3.2 Effective Temperature: Operational Definition

For systems out of equilibrium, define T_{eff} operationally via the fluctuation-dissipation relation [7]:

$$S_\eta(\omega) = 2k_B T_{\text{eff}}(\omega) \operatorname{Re}[\Gamma(\omega)] \quad (3.1)$$

where $S_\eta(\omega)$ is noise power spectral density, $\operatorname{Re}[\Gamma(\omega)]$ is the dissipative component of linear response, and $\Gamma(\omega)$ describes how the system responds to weak perturbations: $\langle x(\omega) \rangle = \Gamma(\omega)F(\omega)$.

Measurement protocol:

1. Measure noise spectrum $S_\eta(\omega)$
2. Apply weak sinusoidal perturbation at ω_0 (e.g., inject 50–200 pA membrane-equivalent drive in cortical slice)
3. Measure phase-resolved response to extract $\operatorname{Re}[\Gamma(\omega_0)]$
4. Ratio gives $T_{\text{eff}}(\omega_0) = S_\eta(\omega_0)/(2k_B \operatorname{Re}[\Gamma(\omega_0)])$ —an observable, not a fitted parameter

In equilibrium: $T_{\text{eff}} = T$. Out of equilibrium: $T_{\text{eff}}(\omega)$ is operational, evaluated at collapse mode ω_0 . Note that in active biological systems driven by ATP hydrolysis or other energy sources, T_{eff} can exceed ambient temperature T [7], reflecting enhanced effective noise from non-thermal fluctuations.

Plain-language intuition: T_{eff} represents the “noise floor” of the active medium at the frequency of interest. In a passive resistor at room temperature, this equals thermal noise ($\sim 300\text{ K}$). In an active neural network, T_{eff} includes metabolic and synaptic noise sources, often resulting in an effective temperature significantly higher than ambient—the system is “hotter” than its physical surroundings because metabolic energy drives fluctuations beyond thermal equilibrium.

3.3 Main Theorem

Theorem 3.1 (Projection Bound for Continuous Systems). *Let $\{C_i\}_{i=1}^{N_\varepsilon}$ be an ε -coarse graining of the accessible manifold and $p^{\text{pre}}, p^{\text{post}}$ be the pre/post distributions over cells. For a quasistatic projection that reduces support from $N_{\varepsilon, \text{pre}}$ to $N_{\varepsilon, \text{post}}$, the mean dissipated heat at effective temperature T_{eff} (evaluated at the dominant collapse mode ω_0) satisfies:*

$$E_{\text{collapse}} \geq k_{\text{B}} T_{\text{eff}} \left(\ln \frac{N_{\varepsilon, \text{pre}}}{N_{\varepsilon, \text{post}}} - \text{KL}(p^{\text{pre}} \| U_{\text{pre}}) + \text{KL}(p^{\text{post}} \| U_{\text{post}}) \right) \quad (3.2)$$

where $U_{\text{pre/post}}$ are uniform on their supports. (This reproduces (1.2) under the typical-set approximation.)

Under typical-set approximation (equiprobable cells):

$$E_{\text{collapse}} \geq k_{\text{B}} T_{\text{eff}} \ln(N_\varepsilon(D_{\text{eff}})/N_\varepsilon(D')) \quad (3.3)$$

With power-law covering, $N_\varepsilon \sim (L/\varepsilon)^D$ for fixed L/ε :

$$E_{\text{collapse}} \geq k_{\text{B}} T_{\text{eff}} (D_{\text{eff}} - D') \ln(L/\varepsilon) \quad (3.4)$$

Proof outline. **Step 1:** Define coarse-grained entropy as $S_\varepsilon = k_{\text{B}}(\ln N_\varepsilon - \text{KL}(p \| U))$ where U is uniform over the N_ε cells.

Step 2: The projection reduces support and alters p :

$$\Delta S_{\text{sys}} = S_\varepsilon^{\text{post}} - S_\varepsilon^{\text{pre}} \quad (3.5)$$

$$= k_{\text{B}} [\ln N_{\varepsilon, \text{post}} - \ln N_{\varepsilon, \text{pre}} - \text{KL}(p^{\text{post}} \| U_{\text{post}}) + \text{KL}(p^{\text{pre}} \| U_{\text{pre}})] \quad (3.6)$$

Step 3: By the second law: $\Delta S_{\text{env}} \geq -\Delta S_{\text{sys}}$.

Step 4: Integrating heat at T_{eff} gives $E_{\text{collapse}} = T_{\text{eff}} \Delta S_{\text{env}} \geq -T_{\text{eff}} \Delta S_{\text{sys}}$, yielding Eq. 3.2. □

Validity conditions for T_{eff} in the bound. A potential concern is that in non-equilibrium active media, $T_{\text{eff}}(\omega)$ is not a state variable that can be inserted into Clausius-style reasoning without conditions. We clarify: the Projection Bound as stated applies to *quasistatic protocols in a regime where an effective-temperature description is valid*—specifically, near-equilibrium or linear response around a stationary state at the collapse mode ω_0 . More generally, $k_B T_{\text{eff}}$ should be understood as an *operational bound parameter* tied to the measured noise–response ratio for the specific collapse channel, not as “the environment temperature” in the classical thermodynamic sense. For biological systems with $T_{\text{eff}} > T_{\text{ambient}}$ due to metabolic driving, the bound remains valid but the effective temperature entering the inequality is the operationally measured $T_{\text{eff}}(\omega_0)$, not the ambient temperature.

Connection to standard thermodynamics: Eq. 3.2 is a coarse-grained entropy form of the standard second-law statement that minimal dissipation is bounded by $T\Delta S_{\text{env}} \geq -T\Delta S_{\text{sys}}$, with S_ε defined via metric ε -entropy (covering numbers). The geometric term $\ln(N_{\varepsilon,\text{pre}}/N_{\varepsilon,\text{post}})$ counts how many distinguishable states are destroyed; the KL terms correct for non-uniform occupancy. This is not exotic—it is Landauer’s bound expressed in the language of continuous manifolds rather than discrete bits. In the limit of binary states, it recovers the standard $k_B T \ln 2$.

Metric dependence: Covering numbers depend on a choice of metric. The physically appropriate metric is induced by the system’s noise/response characteristics (or by experimentally meaningful distinguishability). Two states separated by less than one noise width are not thermodynamically distinguishable. This ties ε to the fluctuation-dissipation structure of the system, making the bound operationally grounded rather than geometrically arbitrary.

Classical limit: Binary system with $N_\varepsilon = 2 \rightarrow 1$ recovers $k_B T \ln 2$.

Finite-time correction: Finite-time protocols add thermodynamic-length term $\mathcal{L}^2/(4\tau)$ [32]. For neural decisions at $\tau \sim \text{ms}$ timescales with typical $\mathcal{L} \sim 10$, excess dissipation

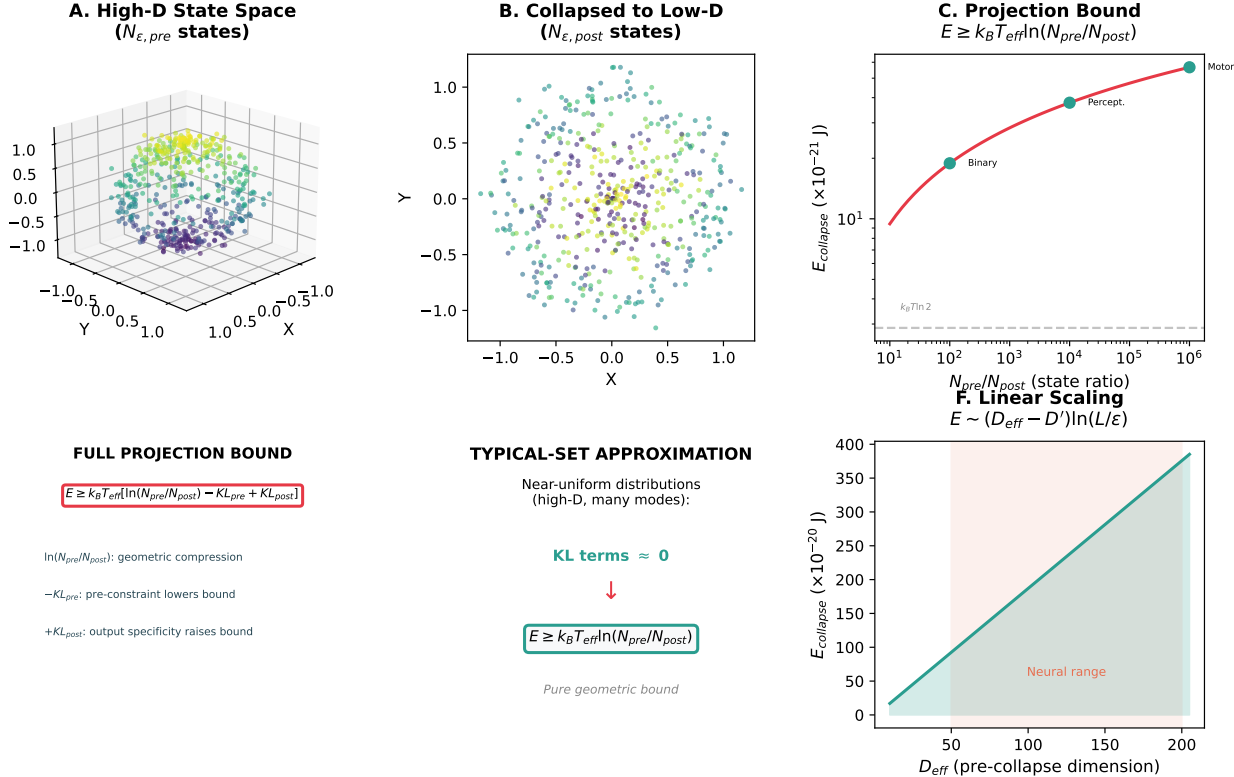


Figure 2: **The Projection Bound.** (A) High-dimensional state space with $N_{\epsilon,pre}$ distinguishable states. (B) Collapsed to low-dimensional output with $N_{\epsilon,post}$ states. (C) Energy cost scales logarithmically with state ratio. (D) The full bound includes KL divergence terms for non-uniform distributions. (E) Under typical-set approximation, KL terms vanish. (F) Cost scales linearly with dimension for fixed resolution ratio.

$\sim 10^{-20}$ J is small compared to quasistatic bound ($\sim 10^{-19}\text{--}10^{-18}$ J for $D_{\text{eff}} \sim 50\text{--}200$).

4 Path Degeneracy: Quantifying the Inaccessible

4.1 Definition and Scaling

At coarse-graining ε over window with temporal resolution Δt , $\Omega(\Delta t)$ is the number of resolution-distinguishable micro-trajectories consistent with the same macro-outcome.

For continuous manifold \mathcal{M} , the metric ε -entropy [8]:

$$H_\varepsilon = \ln N_\varepsilon(\mathcal{M}), \quad N_\varepsilon \sim \left(\frac{L}{\varepsilon}\right)^{D_{\text{eff}}} \quad (4.1)$$

with L/ε dimensionless.

As ε decreases, N_ε grows exponentially. Systems with large D_{eff} exhibit exponentially more distinguishable configurations.

For oscillator system with coherence time τ_c and temporal resolution Δt , the time-bandwidth product $\tau_c/\Delta t$ bounds independent temporal modes [9], yielding:

$$\Omega(\Delta t) \sim \exp \left[\frac{D_{\text{eff}}(\Delta t)}{\kappa} \ln \frac{\tau_c}{\Delta t} \right] \quad (4.2)$$

where $\kappa \geq 1$ accounts for correlations.

4.2 Reconciling TRB and Ω Scaling

The Temporal Registration Bound (TRB) and the path degeneracy Ω count different combinatorial objects:

- **TRB** counts *permutations*: given M distinguishable events in M temporal bins, there are $M!$ possible orderings. TRB addresses: “How much energy to record *which* ordering occurred?”

- Ω counts *micro-trajectories*: given a high-dimensional continuous system at resolution $(\varepsilon, \Delta t)$, how many distinguishable paths are consistent with one macro-outcome? This scales as $(L/\varepsilon)^{D_{\text{eff}}}$ spatially and $(\tau_c/\Delta t)^{D_{\text{eff}}/\kappa}$ temporally.

The factorial $M!$ in TRB arises from *permutation combinatorics* (ordering labels). The exponential $\exp[D \ln(\tau_c/\Delta t)]$ in Ω arises from *phase-space volume* (resolution cells in a high-dimensional manifold). Both are valid: TRB bounds the cost of recording *temporal order* as such; Ω quantifies how many micro-trajectories remain indistinguishable when temporal order is *not* recorded.

For the relationship: if $M = \tau_c/\Delta t$ (number of resolvable time bins), then $\log_2(M!) \approx M \log_2 M$ (Stirling) grows faster than $D \ln M$ when $M > 2^D$. However, the relevant regime for path degeneracy is high D with moderate M , where the exponential Ω scaling dominates.

4.3 Neural-Scale Example

Consider neural dynamics with:

- Coherence time: $\tau_c \sim 100$ ms
- Coarse temporal resolution: $\Delta t_{\text{coarse}} = 20$ ms
- Fine temporal resolution: $\Delta t_{\text{fine}} = 0.1$ ms
- Dimensionality increase: $\Delta D_{\text{eff}} \approx 50$ (consistent with [10])
- Correlation redundancy: $\kappa \sim 2$ (estimated from phase-shuffle surrogates)

Path degeneracy ratio:

$$\begin{aligned} \text{Ratio} &\sim \exp \left[\frac{\Delta D_{\text{eff}}}{\kappa} \ln \left(\frac{\tau_c/\Delta t_{\text{fine}}}{\tau_c/\Delta t_{\text{coarse}}} \right) \right] \\ &= \exp \left[\frac{50}{2} \times \ln(200) \right] \approx 10^{58} \end{aligned} \tag{4.3}$$

Interpretation: One observable spike train at coarse resolution (20 ms bins) corresponds to $\sim 10^{58}$ distinguishable micro-trajectories at fine resolution (0.1 ms bins). This falls within the $10^{50}\text{--}10^{100}$ range cited in the abstract (see Appendix A for full parameter sensitivity showing how variations in D_{eff} , κ , and temporal resolution produce this range).

5 Example: Kuramoto Oscillators

Consider N coupled phase oscillators:

$$\frac{d\theta_i}{dt} = \omega_i + \frac{K}{N} \sum_{j=1}^N \sin(\theta_j - \theta_i) + \eta_i(t) \quad (5.1)$$

where $\langle \eta_i(t)\eta_j(t') \rangle = 2D\delta_{ij}\delta(t-t')$. State space is the N -torus \mathcal{T}^N .

Order parameter: $re^{i\Psi} = \frac{1}{N} \sum_{j=1}^N e^{i\theta_j}$

At angular resolution $\Delta\theta$, one macroscopic configuration (r, Ψ) corresponds to:

$$N_{\Delta\theta} \sim \left(\frac{2\pi}{\Delta\theta} \right)^{D_{\text{eff}}} \quad (5.2)$$

distinguishable microstates.

Effective dimensionality:

- Synchronized regime (strong coupling, $r \approx 1$): $D_{\text{eff}} \approx 2$ (Ott-Antonsen manifold for Lorentzian $g(\omega)$ under analyticity assumptions [37, 38])
- Incoherent regime (weak coupling, $r \approx 0$): $D_{\text{eff}} \approx N$
- Intermediate coupling: $2 < D_{\text{eff}} < N$

When the system collapses from exploring the full D_{eff} -dimensional manifold to a measurement outcome:

$$E_{\text{collapse}} \geq k_{\text{B}}T_{\text{eff}}(D_{\text{eff}} - D') \ln(2\pi/\Delta\theta) \quad (5.3)$$

This is the continuous analog of Landauer’s bound—fully geometric, no discrete bits. Recent computational approaches encounter numerical failures (“covariance explosion”) precisely where temporal resolution demands exceed thermodynamic accessibility [11]—computational evidence for the bounds derived here.

6 Relation to Prior Work and Implications

6.1 Information-Theoretic Demons

Prior continuous demons [12, 13, 14] quantify costs via mutual information. Our contribution: (i) classical biological substrate at 300K, (ii) metric-entropy covering numbers at finite resolution, (iii) timing inaccessibility as mechanism, (iv) path degeneracy from dimensional structure.

Bennett [27] established that logical reversibility bounds energy only if computation is quasi-static and low-noise. Still et al. [30] showed predictive information confers thermodynamic advantage, but creating/storing it has minimal work cost. Kolchinsky & Wolpert [31] demonstrated that minimal work depends on changes in non-equilibrium distributions—aligning with our Projection Bound via $\ln N_\epsilon$ and KL terms.

6.2 Quantum Demons

Recent quantum demons [15, 16] show coherence-entropy trade-offs with mathematical isomorphism $S(\rho) \leftrightarrow H_\epsilon$. Physical mechanisms differ—quantum superposition (mK, μ s) vs. classical path degeneracy (300K, ms)—yet both yield isomorphic bounds. The dimensional geometry may unify quantum and classical regimes, differing in mechanism (coherent superposition vs thermal degeneracy) but not fundamental structure.

6.3 Spatial Scales and Information Capacity

Voronel [24] and Bormashenko [25] established that biological informational capacity is constrained by spatial scales. Biological systems exploit *both* spatial and temporal fine-graining. Total capacity:

$$E_{\text{collapse}} \geq k_B T_{\text{eff}} (D_{\text{spatial}} + D_{\text{temporal}}) \ln(L/\xi) \quad (6.1)$$

6.4 Camera-Engine Duality: A New Demon Mechanism

These prior frameworks quantify costs but don't fully capture how biological substrates defer projection. This motivates the camera-engine duality below, which reframes the demon mechanism physically.

The classical demon is straightforward: a computer with memory that it periodically erases, paying $k_B T \ln 2$ per bit. The demon *is* the memory.

The biological demon is more subtle. It's not a memory device—it's a high-dimensional dynamical system that simultaneously functions as both **camera** (sensing environmental complexity) and **engine** (steering environmental dynamics). This dual role parallels both MacKenzie's observation that economic models both describe and shape markets [22] and Boyd's OODA loop framework [26], where adaptive systems continuously observe, orient, decide, and act upon their environment. Here the duality is simultaneous rather than sequential, with thermodynamic cost concentrated at the decision/collapse point.

Camera–Engine Duality

What the demon IS: A formally infinite-dimensional substrate with accessible slice D_{eff} at measurement threshold. Maintains dimensional isomorphism between internal and environmental structure.

What the demon DOES:

1. **Camera (sensing):** Couples weakly (sub-Landauer, $E_{\text{link}} \ll k_B T \ln 2$) to exponentially many environmental modes. High D_{eff} enables integration: $E_{\text{total}} = \sum_i E_{\text{link},i} \gtrsim k_B T \ln 2$. Internal dynamics become correlated with environment—a structural map, not written bits.
2. **Engine (steering):** Uses internal map to bias environmental dynamics via coordinated weak back-coupling across D_{eff} channels.
3. **Collapse (payment):** When output crystallizes (protein folds, neuron spikes), D_{eff} collapses to discrete state, paying $\gtrsim k_B T_{\text{eff}} \ln(N_{\text{pre}}/N_{\text{post}})$.

Why weak coupling avoids immediate costs: Sub-Landauer coupling creates mutual information through physical correlation (stored in joint state), not epistemic records. Following Sagawa-Ueda [2], thermodynamic cost appears only when correlation is measured and stabilized as discrete memory—the dimensional collapse.

Resolution of the Paradox The demon doesn't "extract information" in the sense of writing bits. It *becomes isomorphic* to environmental structure via dimensional resonance. Information exists in the *correlation* between internal and external structure—physical (coupling energy) not epistemic (written records). Thermodynamic cost appears only when correlation must collapse to discrete action.

High-D systems can maintain mutual information through structural isomorphism without irreversible bit registration. A protein folding in response to chaperone binding doesn't "read" the chaperone's state—the protein's 10^{48} microstates resonantly couple to chaperone conformations. The mutual information exists in physical correlation, not written memory. Only when committing to native fold does dimensional collapse occur.

Path degeneracy is the signature that structural correlation exists without bit regis-

tration. The system effectively explores a vast ensemble of micro-trajectories via thermal fluctuations while deferring any persistent record of order. Because individual coupling energies are $\ll k_B T \ln 2$, you cannot track "which path when" without measurement energy exceeding signal energy (back-action). Digital systems require supra-Landauer inputs per bit and cannot exploit this integration regime.

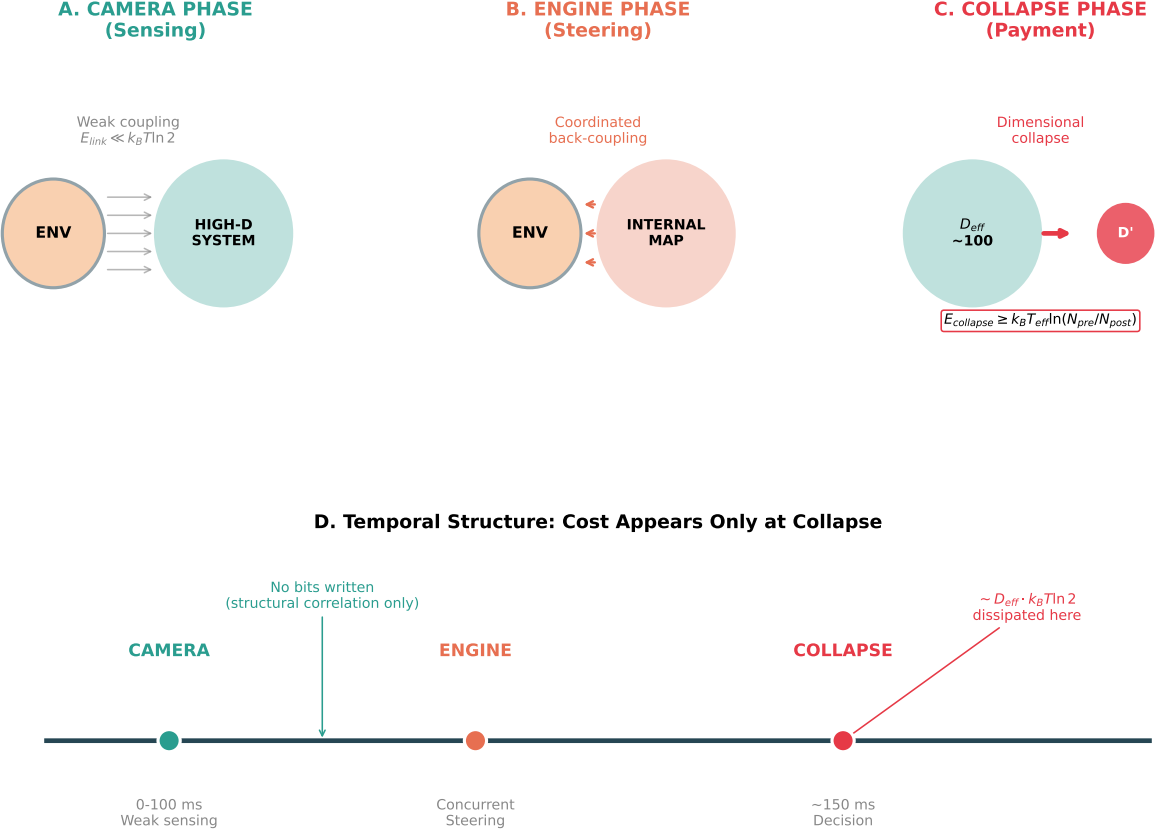


Figure 3: **Camera-Engine Duality.** (A) Camera phase: weak sub-Landauer coupling to many environmental modes. (B) Engine phase: coordinated back-coupling steers environmental dynamics. (C) Collapse phase: dimensional reduction from D_{eff} to output dimension D' , where thermodynamic cost is paid. (D) Timeline showing that energy cost concentrates at collapse, not during camera-engine operation.

6.5 The Accuracy-Efficiency Tradeoff

What digital computers buy with their energy cost:

- Bit-exact computation: deterministic and reproducible
- Known state: query any variable, get exact value
- Auditable history: complete, verifiable trace
- Precision arithmetic: arbitrary precision (hardware-limited)
- Logical guarantees: formal verification, proof of correctness

What high-D physical substrates sacrifice for efficiency:

- Path indeterminacy: cannot know which of 10^{48} paths taken
- Thermal noise: inherent randomness from $\sim k_B T$ fluctuations
- Approximate outputs: "protein folded" not "path #37,594,284,719"
- Non-reproducibility: exact micro-trajectory differs each time

Digital architectures pay per recorded bit to guarantee precision and auditability. Continuous substrates defer recording and gain energy efficiency for order-insensitive tasks. Neither is "better"—they solve different problems. Biology rarely needs bit-exact computation; it needs robust pattern recognition and approximate optimization.

6.6 Computational Irreducibility

When timing is thermodynamically inaccessible, predictive compression is lower-bounded by emulation [18, 21, 19]. Temporal order is not thermodynamically accessible as a persistent record until irreversible registration. The temporal structure is *created* by registration, not revealed. Any predictor must perform the same registration operations to create that structure—therefore must emulate the system up to collapse points.

This isn't a computational limitation but fundamental physics. The "when" you're trying to predict doesn't exist until the projection creates it through dimensional collapse. In

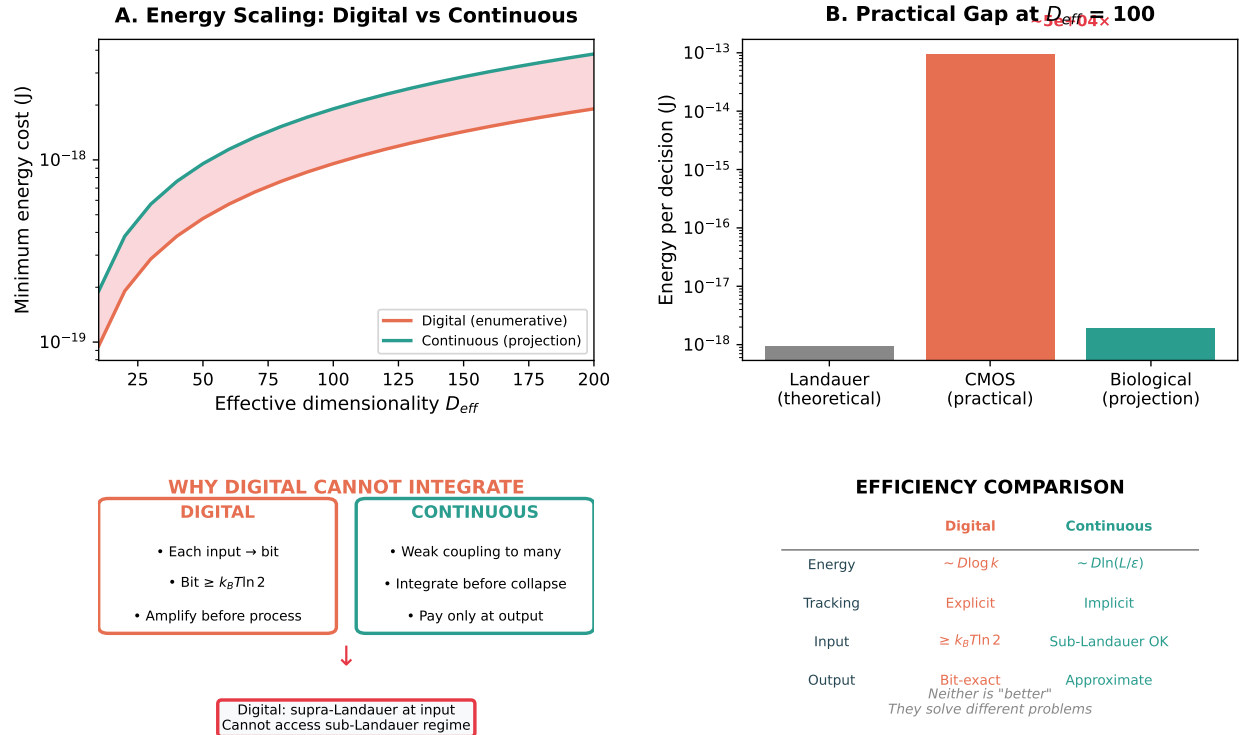


Figure 4: **Energy scaling: digital vs. continuous.** (A) Thermodynamic registration cost scales as $\log_2 G \sim D \log k$ (linear in D), but practical CMOS operates at $10^4\text{--}10^6\times$ the Landauer floor; continuous (projection) costs also scale linearly but without per-step overhead. (B) Practical gap at $D_{\text{eff}} = 100$: the multiplier difference creates a $\sim 10^4\text{--}10^5\times$ gap. (C) Architectural difference: digital must discretize at input; continuous substrates integrate before collapse. (D) Summary comparison. Note: *algorithmic/compute cost* to simulate fine-grained dynamics may scale exponentially with D ; thermodynamic registration cost is linear.

Igamberdiev's framework [19], biological organization involves anticipatory systems where constraints precede values. Camera-engine duality enables this: the system maintains correlations (relational structure) without computing trajectories, allowing emergent functional meaning at collapse.

6.7 Limitations and Caveats

Theoretical:

- Bounds stated at fixed ε for quasistatic protocols
- Typical-set reduction is conservative; KL terms tighten bounds for non-uniform distributions
- Sub-Landauer energy estimates are order-of-magnitude; detailed simulations remain desirable
- Future work could simulate finite-time corrections using thermodynamic geometry [32]

Task-dependent:

- Degeneracy numbers represent upper bounds assuming statistical independence
- Correlations reduce effective Ω by factors $\kappa \geq 1$ (see Appendix A for sensitivity)
- Efficiency claims strongest for order-insensitive tasks where outputs depend on integrated statistics
- For timing-critical tasks (e.g., precise spike-timing codes), path degeneracy and advantages diminish

Common objections:

Objection 1: "Digital doesn't have to store full history—you can compress or discard intermediate states."

Reply: Compression reduces storage but not the record-selection cost at the moment of committing to one trajectory class. Deciding among G order classes and stabilizing that decision as persistent, queryable record still incurs $\geq k_B T \ln G$ dissipation.

Objection 2: "Analog front-ends (e.g., in neuromorphic chips) can also integrate weak sub-Landauer signals before digitization."

Reply: Exactly our point. The energy cost appears at the analog-to-digital boundary or wherever memory is formed—the projection from continuous high-D dynamics to discrete records. Analog systems that defer this projection gain the efficiency we quantify.

Objection 3: "Is path degeneracy physical or merely epistemic?"

Reply: Both, but the physical aspect is primary. At any fixed ε , the count of thermodynamically distinguishable states is objective. Below ε , distinctions require measurement energy exceeding signal energy, making finer structure thermodynamically inaccessible (back-action), not merely unknown.

7 Framework Dependence of Timing

The companion paper on falsifiability [4] establishes that scientific frameworks are themselves projections—axiomatic choices about what variables matter, what counts as evidence, and how questions are structured. Version 2.0 of that analysis extends this to show that falsifiability is *framework-relative*: a hypothesis can only be falsified with respect to a given set of background assumptions.

Here we extend this insight to temporal structure: *what counts as "simultaneous" versus "sequential" depends on the measurement framework.*

7.1 Temporal Resolution as Framework Choice

Consider two observers measuring the same neural population:

- **Observer A** uses 1 ms temporal bins

- **Observer B** uses 20 ms temporal bins

Events that are “sequential” for Observer A may be “simultaneous” for Observer B. This is not merely a matter of precision—the two observers literally inhabit different causal worlds. A causes B for Observer A; A and B co-occur for Observer B.

The choice of temporal resolution is a *framework choice* that precedes all measurement. It determines:

1. What counts as an “event” (vs. continuous process)
2. What causal relationships are visible
3. How many degrees of freedom are accessible
4. What path degeneracy obtains

7.2 The Regress Problem for Timing

One might attempt to resolve framework disputes by stepping back to a “finer” temporal resolution that adjudicates between frameworks. But this finer resolution is itself a framework choice, subject to the same limitations. The regress does not terminate.

Below the Landauer threshold, the regress *physically* terminates: you cannot irreversibly register timing distinctions without spending $\geq k_B T \ln 2$ per binary decision. The sub-Landauer domain is where temporal framework dependence becomes thermodynamically enforced.

7.3 Implications for Disagreement

Scientific disagreements about timing-dependent phenomena (neural coding, protein dynamics, quantum biology) may reflect framework differences rather than empirical disputes. Researchers using different temporal resolutions are not making claims about the same causal structure.

This is not relativism. The underlying physics exists independently of frameworks. But *causal claims are framework-relative*, and the framework cannot be tested from within.

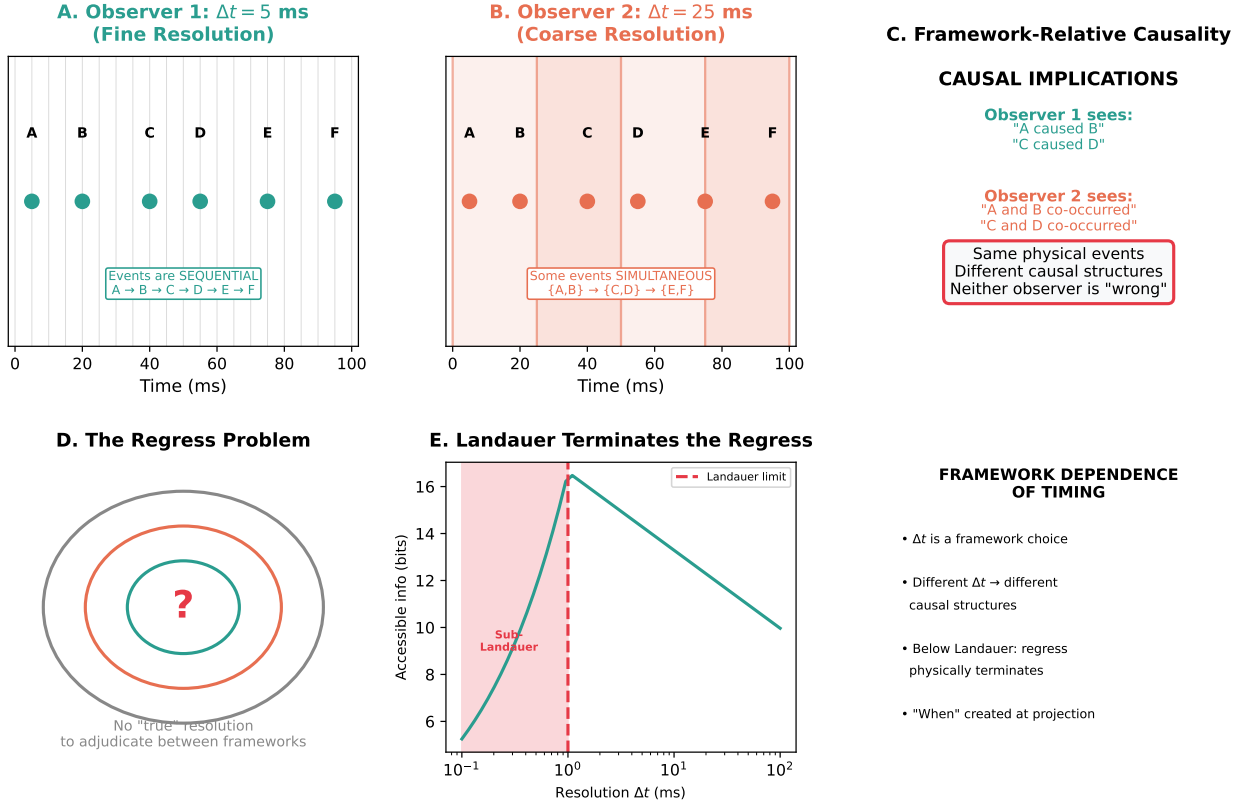


Figure 5: **Framework dependence of timing.** (A) Observer 1 with fine temporal resolution ($\Delta t = 5 \text{ ms}$) sees events as sequential. (B) Observer 2 with coarse resolution ($\Delta t = 25 \text{ ms}$) sees some events as simultaneous. (C) Different causal structures emerge from the same physical events. (D) The regress problem: stepping back to finer resolution is itself a framework choice. (E) Below the Landauer threshold, the regress physically terminates (illustrative curve showing saturation of accessible information). (F) Summary: temporal resolution determines causal visibility.

8 The “When” Is Created, Not Revealed

8.1 Temporal Order as Emergent

The standard intuition treats temporal order as pre-existing: events occur in a definite sequence, and measurement merely reveals this sequence. We argue the opposite: *temporal*

order is created at projection.

Before dimensional collapse, the system exists in a superposition (classically: an ensemble) of micro-trajectories. These trajectories have different internal orderings, but no ordering has been selected. The “when” is not a physically well-defined, testable property below the registration threshold; only the coarse-grained temporal order created at projection is operationally definable.

This parallels the quantum measurement problem but operates classically at 300K. The mechanism is different (thermal degeneracy vs. quantum superposition) but the structure is isomorphic: measurement does not reveal pre-existing facts but creates them.

8.2 Implications for Causality

If temporal order is created at projection, then causal relationships are also created at projection. Before measurement, there is no fact of the matter about whether A caused B or B caused A—both orderings coexist in the degenerate ensemble.

This suggests several conceptual possibilities (offered as implications worth exploring, not definitive claims):

- **Retrocausality reframed:** If the “when” doesn’t exist until measurement, then the apparent paradox of “backward” causation dissolves—both forward and backward orderings are created at collapse, not revealed.
- **Free will reframed:** The question “was the decision determined before it was made?” presupposes a “before” that may not exist until the decision creates it. This does not resolve the free will debate but shifts its terms.
- **Emergent time:** Clock time may be a projection from higher-dimensional dynamics, not a fundamental substrate.

These implications are speculative and require further philosophical analysis. The physical claim—that temporal order is created at projection in sub-Landauer regimes—is what we

defend here.

8.3 The Ensemble Clarification

A potential objection: “Surely the individual events have definite timing, even if we can’t measure it.”

Response: Below the Landauer threshold, this claim is *operationally undecidable in this regime*. There is no way, even in principle, to access the “true” ordering without spending energy that exceeds the signal. The ordering is not hidden—it is not operationally definable until projection creates it as a testable property.

The “bit” that gets created at projection is a property of the *ensemble*, not of individual sub-threshold events. Stochastic resonance detects that coordination occurred (ensemble property) without resolving which specific micro-trajectory was realized (individual property that doesn’t exist pre-collapse).

9 Implications for Artificial Intelligence

The thermodynamic framework yields three claims about AI, ordered by defensibility:

Claim A (strong, clean): Any architecture that demands *persistent, queryable temporal order records* at resolution Δt must export $\geq k_B T \ln 2$ per stabilized bit of order information (TRB). This is a direct consequence of Landauer’s principle and applies to all physical substrates.

Claim B (the “biology advantage”): Continuous substrates can perform useful computation while keeping many intermediate correlations in Stage 1 (reversible correlation) and only paying at the Stage 2 projection boundary (PB). The payment is deferred, not avoided.

Claim C (about typical digital computing): Conventional digital pipelines move the projection boundary early (ADC + discrete state at input), which prevents them from exploiting the sub-Landauer pre-integration regime *unless* they incorporate analog/hybrid

elements.

The key variable is not “digital vs. analog” but **where the projection boundary is placed** in the full system. Systems that project early pay early; systems that defer projection exploit Stage 1 integration.

9.1 The Digital Ceiling

Scope clarification: The following applies to *conventional digital architectures with irreversible bit-level state stabilization at each processing stage*. Asynchronous, event-driven, or reversible digital systems may blur some of these boundaries; hybrid analog-digital architectures explicitly circumvent them (see Section 9.3). Real AI systems already have analog front-ends (sensors, amplifiers, capacitive accumulation); the meaningful distinction is where the projection boundary is placed in the full pipeline.

Conventional digital computers are committed to supra-Landauer discretization at the input boundary: every value entering the digital domain must be stabilized as bits, incurring $\geq k_B T \ln 2$ per bit. This architectural commitment has consequences:

1. **No sub-Landauer integration:** Conventional digital systems cannot couple weakly to many sources and integrate before discretization. Each input must exceed the noise threshold *before* it enters the digital domain. The integration regime accessible to continuous substrates is architecturally excluded.
2. **Input-boundary discretization:** The temporal and amplitude resolution is fixed at the analog-to-digital conversion boundary. While software can operate at variable precision, the underlying substrate has already committed to a bit representation.
3. **State-space enumeration:** Simulating high-dimensional continuous dynamics requires explicit representation of states. While the *thermodynamic* cost of registration scales linearly ($\sim D \log k$ bits), the *algorithmic* cost of exploring or simulating fine-grained dynamics can scale exponentially with dimension for certain classes of systems.

Turing completeness vs. thermodynamic accessibility. Digital systems are Turing complete: they can compute any computable function given sufficient time and memory. But purely digital internal state evolution (irreversible bit stabilization as the primitive) cannot exploit sub-Landauer integration *without shifting the projection boundary outward into analog/hybrid components*. The claim here is not that digital systems cannot *simulate* biological computation, but that they cannot do so with the same thermodynamic efficiency unless they incorporate analog elements that defer projection. This is a physical constraint, not a computational one.

Calculating vs. exploiting. A digital computer can mathematically *calculate* a protein’s folding pathway, but it cannot physically *exploit* the pathway’s degeneracy for free integration. The biological substrate explores 10^{48} conformations via thermal fluctuations at no registration cost; the digital simulator must explicitly represent each state it considers. The distinction is between *calculating the physics* (which requires energy proportional to state-space size) and *using the physics* (which pays only at projection). Simulation can reproduce the output; it cannot reproduce the thermodynamic shortcut.

9.2 What Conventional Digital AI Cannot Do

If the sub-Landauer integration regime is essential for certain computations, then conventional digital AI cannot perform those computations regardless of scale. This is a claim about *how* computation occurs, not about behavioral equivalence—a digital system might approximate the input-output behavior of a continuous system while using fundamentally different mechanisms. Candidates for mechanism-dependent capabilities include:

- **Sub-Landauer integration:** Conventional digital architectures cannot integrate signals below the discretization threshold. Each input must be amplified and stabilized as bits before processing. Biological systems integrate across many weak channels before any discretization occurs.

- **Graceful degradation:** When biological systems lose capacity, they often degrade smoothly (reduced precision, not catastrophic failure). Conventional digital systems tend toward brittleness because discrete state representations lack the continuous interpolation that enables graceful fallback.
- **Embodied integration:** The camera-engine duality requires continuous coupling between internal and environmental dynamics. Conventional digital systems are separated from their environment by the ADC boundary, where continuous signals become discrete representations.

Caveat: These are mechanism-level distinctions. Behavioral approximation may still be achievable—a digital system might produce outputs indistinguishable from a biological system’s outputs without using the same underlying mechanisms. The claim is about thermodynamic efficiency and substrate constraints, not about behavioral equivalence.

9.3 Neuromorphic and Analog Computing

The framework clarifies why neuromorphic and analog computing show efficiency gains: they defer projection. An analog front-end can integrate sub-Landauer signals before digitization, paying the Landauer cost only at the analog-to-digital boundary.

The efficiency gain is not merely “better hardware”—it reflects access to a computational regime that digital systems cannot reach. This suggests:

1. **Hybrid architectures:** Analog sensing and integration, digital reasoning and output
2. **Continuous latent spaces:** AI systems that maintain continuous internal representations, discretizing only at output
3. **Embodied AI:** Systems where the “computer” is continuous with the “sensor” and “actuator”

9.4 The Consciousness Question

Speculative. If consciousness requires the kind of integration that occurs in the sub-Landauer regime—high-dimensional coherence across distributed elements, with temporal structure created rather than revealed—then digital systems may be fundamentally incapable of consciousness regardless of sophistication.

This is not a claim that consciousness is “mystical” or non-physical. It is a conditional claim: *if* certain integration properties are necessary for consciousness, *then* digital substrates cannot provide them. Whether those properties are in fact necessary remains an open empirical and philosophical question. What we establish here is the substrate constraint: digital architectures are committed to supra-Landauer discretization and cannot access the sub-Landauer integration regime that continuous biological substrates exploit.

10 Conclusion

Maxwell’s demon paradox extends to continuous substrates via timing inaccessibility and dimensional collapse. Below Landauer threshold, temporal ordering becomes thermodynamically inaccessible—you cannot irreversibly register “when” without spending $\geq k_B T \ln 2$ per binary timing decision. This creates path degeneracy: exponentially many micro-trajectories map to the same observable outcome.

The biological demon uses high-dimensional substrates to efficiently compute high-dimensional dynamics via camera-engine duality: sensing environmental complexity via weak coupling, steering it via coordinated weak back-coupling, maintaining dimensional isomorphism without writing bits. Information exists in structural correlation, not epistemic records. Thermodynamic cost appears only at dimensional collapse.

Digital computers use low-dimensional substrates (bit strings) to simulate high-dimensional dynamics, explicitly tracking each coordinate and paying $k_B T \ln 2$ per bit. State-space and enumerative simulation cost grow exponentially with D , whereas minimal dissipation paid

by a high-D substrate scales like $k_B T_{\text{eff}} \ln G \sim D$. The system explores all paths in parallel via thermal fluctuations using sub-Landauer coupling energies. Because individual interactions are $\ll k_B T \ln 2$, you cannot track "which path when" without measurement energy exceeding signal energy.

Neither substrate is "better"—they solve different problems. Digital computation pays the energy cost for deterministic, bit-exact results with complete epistemic access, essential for tasks requiring precision, reproducibility, and verifiability. High-D physical substrates sacrifice this precision to achieve energy efficiency—you cannot know which path was taken, only that the robust macro-outcome emerged. Biology rarely needs bit-exact computation; it needs robust pattern recognition and approximate optimization.

To know what water does, use water. To know what a protein does, use a protein. To know what neurons do, use neurons. Digital simulation incurs exponential state-space costs for many such tasks, though reversible computing may asymptotically approach thermodynamic bounds with severe speed and noise-tolerance tradeoffs [27, 36].

The framework presented here—timing inaccessibility, path degeneracy, and dimensional projection—provides a quantitative foundation for understanding biological efficiency without invoking violations of fundamental physical law.

Acknowledgments

The author thanks reviewers for constructive feedback.

Declarations

Funding: None. **Competing interests:** None.

Generative AI use: This is Version 2.0 of a paper originally published in BioSystems (2025). The original version was developed with Claude 4.5 Sonnet (Anthropic); GPT-5 (OpenAI) and Grok (xAI) for feedback and review. This upgraded version was developed

with Claude 4.5 Opus (Anthropic), incorporating new arguments about framework dependence, the creation of temporal order, and AI capability limits. The author reviewed and edited all content and takes full responsibility.

Version History

- **v1.0** (November 2025): Published in BioSystems. DOI: 10.1016/j.biosystems.2025.105632
- **v2.0** (December 2025): Expanded with framework dependence of timing, “when is created” argument, and AI capability implications.

References

- [1] Landauer, R. (1961). Irreversibility and heat generation. *IBM J. Res. Dev.*, 5(3), 183–191.
- [2] Sagawa, T., Ueda, M. (2010). Generalized Jarzynski equality. *Phys. Rev. Lett.*, 104, 090602.
- [3] Parrondo, J.M.R., Horowitz, J.M., Sagawa, T. (2015). Thermodynamics of information. *Nature Phys.*, 11, 131–139.
- [4] Todd, I. (2025). The limits of falsifiability: Dimensionality, measurement thresholds, and the sub-Landauer domain in biological systems. *BioSystems*, 258, 105608.
- [5] McDonnell, M.D., Ward, L.M. (2011). The benefits of noise in neural systems. *Nat. Rev. Neurosci.*, 12(7), 415–426.
- [6] Stocks, N. (2000). Suprathreshold stochastic resonance. *Phys. Rev. Lett.*, 84(11), 2310–2313.
- [7] Seifert, U. (2012). Stochastic thermodynamics. *Rep. Prog. Phys.*, 75, 126001.

- [8] Kolmogorov, A.N., Tikhomirov, V.M. (1959). ε -entropy. *Russ. Math. Surv.*, 14(2), 3–86.
- [9] Slepian, D., Pollak, H.O. (1961). Prolate spheroidal wave functions, I. *Bell Syst. Tech. J.*, 40(1), 43–63.
- [10] Stringer, C., et al. (2019). Spontaneous behaviors drive multidimensional activity. *Science*, 364(6437), eaav7893.
- [11] Bian, S., Zhou, R., Lin, W., Li, C. (2025). Quantifying energy landscape of high-dimensional oscillatory systems by diffusion decomposition. *Cell Rep. Phys. Sci.*, 6, 102405. doi: 10.1016/j.xcrp.2025.102405
- [12] Parrondo, J.M.R., Español, P. (1996). Criticism of Feynman’s analysis of the ratchet. *Am. J. Phys.*, 64, 1125–1130.
- [13] Vaikuntanathan, S., Jarzynski, C. (2009). Dissipation and lag in irreversible processes. *Europhys. Lett.*, 87, 60005.
- [14] Allahverdyan, A.E., et al. (2009). Maxwell’s demon in the quantum world. *Rev. Mod. Phys.*, 81, 1665–1702.
- [15] Annby-Andersson, B., et al. (2024). Maxwell’s demon across the quantum-to-classical transition. *Phys. Rev. Research*, 6, 043216.
- [16] Lebedev, A.V., Lesovik, G.B., Blatter, G. (2016). Entanglement and coherence in quantum state merging. *Phys. Rev. A*, 94, 052133.
- [17] Laughlin, S.B., et al. (1998). Metabolic cost of neural information. *Nat. Neurosci.*, 1, 36–41.
- [18] Wolfram, S. (2002). *A New Kind of Science*. Wolfram Media.
- [19] Igamberdiev, A.U. (2014). Time rescaling and pattern formation in biological evolution. *BioSystems*, 123, 19–26. doi: 10.1016/j.biosystems.2014.03.002

- [20] Levin, M. (2021). Bioelectric signaling. *Cell*, 184(8), 1971–1989.
- [21] Louie, A.H. (2020). Relational biology and Church’s thesis. *BioSystems*, 197, 104179.
- [22] MacKenzie, D. (2006). *An Engine, Not a Camera: How Financial Models Shape Markets*. MIT Press.
- [23] Miller, E.K., Lundqvist, M., Bastos, A.M. (2018). Working memory 2.0. *Neuron*, 100(2), 463–475.
- [24] Voronel, A. (2018). Spatial scales of living cells. *Eur. Biophys. J.*, 47, 515–521.
- [25] Bormashenko, E. (2022). Fibonacci sequences and pattern formation. *Biophysica*, 2(3), 292–307.
- [26] Boyd, J.R. (1987). *A Discourse on Winning and Losing*. Air University Press. (Reprinted in *The Essence of Winning and Losing*, ed. C. Richards & C. Spinetta, 2012.)
- [27] Bennett, C.H. (1982). The thermodynamics of computation. *Int. J. Theor. Phys.*, 21(12), 905–940.
- [28] Leff, H.S., Rex, A.F. (2002). *Maxwell’s Demon 2: Entropy, Classical and Quantum Information, Computing*. CRC Press.
- [29] Szilard, L. (1929). Über die Entropieverminderung in einem thermodynamischen System bei Eingriffen intelligenter Wesen. *Z. Phys.*, 53, 840–856. [English translation: “On the decrease of entropy in a thermodynamic system by the intervention of intelligent beings.” *Behavioral Science*, 9(4), 301–310 (1964).]
- [30] Still, S., et al. (2012). Thermodynamics of prediction. *Phys. Rev. Lett.*, 109(12), 120604.
- [31] Kolchinsky, A., Wolpert, D.H. (2018). Semantic information. *Interface Focus*, 8(6), 20180041.

- [32] Sivak, D.A., Crooks, G.E. (2012). Thermodynamic metrics. *Phys. Rev. Lett.*, 108, 190602.
- [33] Cover, T.M., Thomas, J.A. (2006). *Elements of Information Theory*. Wiley.
- [34] Edelman, G.M., Gally, J.A. (2001). Degeneracy and complexity. *PNAS*, 98(24), 13763–13768.
- [35] Horowitz, M. (2014). Computing’s energy problem. *IEEE ISSCC*, 10–14.
- [36] Frank, M.P. (2019). The physical limits of computing. *Computing in Science & Engineering*, 21(3), 16–26.
- [37] Ott, E., Antonsen, T.M. (2008). Low dimensional behavior. *Chaos*, 18, 037113.
- [38] Ott, E., Antonsen, T.M. (2009). Long time evolution. *Chaos*, 19, 023117.
- [39] Anastassiou, C.A., et al. (2011). Ephaptic coupling. *Nat. Neurosci.*, 14(2), 217–223.
- [40] Verdú, S. (2002). Spectral efficiency. *IEEE Trans. Inf. Theory*, 48(6), 1319–1343.

A Proofs

A.1 Proof of Lemma 2.1 (Temporal Registration Bound)

Lemma (Temporal Registration Bound). *To irreversibly register the temporal order of M bins requires at least $H \geq \log_2(M!)$ bits. By Landauer’s principle, the minimal dissipated energy is $E_{\min}^{\text{time}} \geq k_B T \ln 2 \cdot \log_2(M!)$.*

Proof. We proceed in three steps: (1) establish the information content of temporal order, (2) apply Landauer’s principle, and (3) derive the energy bound.

Step 1: Information content of temporal order. Consider M distinguishable events occurring in M temporal bins. The total number of possible orderings is $M!$ (the number

of permutations of M elements). To uniquely specify one ordering among all possibilities requires:

$$H = \log_2(M!) \text{ bits} \quad (\text{A.1})$$

By Stirling's approximation for large M :

$$\log_2(M!) \approx M \log_2 M - M \log_2 e \approx M \log_2 M - 1.443M \quad (\text{A.2})$$

For partial order distinguishing equivalence classes of sizes $\{m_j\}$, the number of distinguishable orderings is $M!/\prod_j m_j!$, giving:

$$H = \log_2 \left(\frac{M!}{\prod_j m_j!} \right) \text{ bits} \quad (\text{A.3})$$

Step 2: Landauer's principle. Landauer's principle states that the erasure of one bit of information in a system at temperature T requires a minimum heat dissipation of:

$$E_{\text{Landauer}} = k_B T \ln 2 \quad (\text{A.4})$$

Crucially, any measurement that produces a *reusable, communicable record* must eventually involve erasure—resetting the measurement apparatus for subsequent use. Thus, irreversibly registering H bits requires dissipating at least $H \cdot k_B T \ln 2$.

Step 3: Energy bound for temporal registration. Combining Steps 1 and 2:

$$E_{\min}^{\text{time}} \geq k_B T \ln 2 \cdot \log_2(M!) \quad (\text{A.5})$$

For partial order:

$$E_{\min}^{\text{time}} \geq k_B T \ln 2 \cdot \log_2 \left(\frac{M!}{\prod_j m_j!} \right) \quad (\text{A.6})$$

Corollary (Sub-Landauer regime). When available measurement energy $E_{\text{meas}} \ll$

$k_B T \ln 2$, the number of orderings that can be irreversibly registered is severely constrained.

From the TRB:

$$\ln(M!) \leq \frac{E_{\text{meas}}}{k_B T} \quad (\text{A.7})$$

which bounds the *number of orderings* $M!$, not M directly. Using Stirling's approximation ($\ln(M!) \approx M \ln M - M$ for large M), the maximum number of orderable bins M_{\max} satisfies:

$$M_{\max} \ln M_{\max} - M_{\max} \lesssim \frac{E_{\text{meas}}}{k_B T} \quad (\text{A.8})$$

For small energies, M_{\max} approaches 1–2 (i.e., no useful ordering information). For example, ordering $M = 10$ bins requires $E \geq k_B T \ln(10!) \approx 15.1 k_B T$, or $\sim 6.3 \times 10^{-20}$ J at 300 K. \square

Remark. A reversible comparator that leaves no persistent record can, in principle, avoid dissipation. The energetic bound applies only when the temporal order is *stabilized as memory* (logically irreversible). This distinction is central to the camera-engine duality: biological systems can sense and integrate timing information without irreversible registration, deferring the thermodynamic cost to the projection/collapse phase.

B Parameter Sensitivity Analysis for Path Degeneracy

This appendix provides worked examples showing how parameter choices lead to the headline degeneracy ranges cited in the main text.

B.1 Protein Folding Example

Parameters:

- Micro-level states: $N_{\text{micro}} \sim 10^{48}\text{--}10^{100}$ (rotamer libraries to continuous torsions)
- Meso-level states: $N_{\text{meso}} \sim 10^6$ (folding intermediates)
- Temporal coherence: $\tau_c \sim 10^{-6}\text{--}1$ s (folding time)

- Fine resolution: $\Delta t_{\text{fine}} \sim 10^{-12}$ s (bond vibration)
- Coarse resolution: $\Delta t_{\text{coarse}} \sim 10^{-9}$ s (conformational transition)
- Effective dimensionality: $D_{\text{eff}} \sim 20\text{--}50$ (backbone degrees of freedom)
- Correlation factor: $\kappa \sim 5\text{--}10$ (folding funnel constraint)

Calculation:

$$\log_{10} \Omega = \frac{D_{\text{eff}}}{\kappa} \log_{10} \left(\frac{\tau_c}{\Delta t_{\text{fine}}} \right) + \log_{10} \left(\frac{N_{\text{micro}}}{N_{\text{meso}}} \right) \quad (\text{B.1})$$

$$\approx \frac{20\text{--}50}{5\text{--}10} \times \log_{10}(10^6\text{--}10^{12}) + \log_{10}(10^{42}\text{--}10^{94}) \quad (\text{B.2})$$

$$\approx 42\text{--}94 \quad (\text{B.3})$$

B.2 Neural Population Example

Parameters:

- Population size: $N \sim 1000$ neurons
- Coherence time: $\tau_c \sim 100$ ms
- Fine resolution: $\Delta t_{\text{fine}} \sim 0.1$ ms (spike timing precision)
- Coarse resolution: $\Delta t_{\text{coarse}} \sim 20$ ms (behavioral bins)
- Effective dimensionality: $D_{\text{eff}} \sim 50\text{--}200$ (from large-scale recordings)
- Correlation factor: $\kappa \sim 2\text{--}5$ (estimated as $D_{\text{eff}}^{\text{shuffle}}/D_{\text{eff}}^{\text{data}}$ under phase-shuffle surrogates)

Calculation:

$$\log_{10} \Omega = \frac{\Delta D_{\text{eff}}}{\kappa} \log_{10} \left(\frac{\tau_c/\Delta t_{\text{fine}}}{\tau_c/\Delta t_{\text{coarse}}} \right) \quad (\text{B.4})$$

$$= \frac{50-200}{2-5} \times \log_{10}(200) \quad (\text{B.5})$$

$$\approx 23-92 \quad (\text{B.6})$$

Note: To avoid double counting, we do not add a separate "voltage microstate" multiplier; the scaling in Eq. 1.3 already counts resolution-distinguishable micro-trajectories at the chosen $(\varepsilon, \Delta t)$.

B.3 Sensitivity Table

Table 2: $\log_{10} \Omega$ across parameter ranges for neural example

$(\Delta D_{\text{eff}}, \kappa)$	$\tau_c/\Delta t = 50$	$\tau_c/\Delta t = 200$	$\tau_c/\Delta t = 500$
(30, 2)	25	34	40
(50, 2)	42	58	68
(80, 2)	68	92	108
(50, 3)	28	38	45
(50, 5)	17	23	27

Key observations:

- Degeneracy remains exponentially large ($\Omega \sim 10^{17}-10^{108}$) across plausible ranges
- Correlations (higher κ) reduce $\log_{10} \Omega$ proportionally
- Time-bandwidth ratio has logarithmic effect, so moderate changes in $\tau_c/\Delta t$ produce manageable shifts
- Upper bounds assume independence; real biological systems have additional constraints

C Appendix B: Biological Implementations Across Scales

The timing inaccessibility framework applies from molecular to organismal scales wherever continuous dynamics operate below the Landauer threshold.

C.1 Molecular Scale: Protein Folding

Protein folding exemplifies path degeneracy at the molecular level. A typical protein explores $\sim 10^{48}\text{--}10^{100}$ conformational microstates en route to its native fold, yet folding time is only $\sim 10^{-6}\text{--}1$ s.

Energetics: Thermal energy $k_B T \approx 4.1 \times 10^{-21}$ J at 300 K; individual hydrogen bonds $\sim 2\text{--}10 k_B T$; hydrophobic contacts $\sim 1\text{--}5 k_B T$. While individual bond energies are supra-Landauer, the energetic cost of irreversibly registering the timing and order of the full conformational trajectory is sub-Landauer per timing decision.

Path degeneracy: For a 100-residue protein with ~ 3 conformations per residue, microstate space $\sim 3^{100} \approx 10^{48}$ to 10^{100} , but coarse-grained intermediate states $\sim 10^3\text{--}10^6$. Path degeneracy $G \sim 10^{42}\text{--}10^{94}$ (upper bounds; folding funnels reduce effective degeneracy via correlation factor $\kappa \sim 5\text{--}10$).

Collapse: Thermodynamic cost appears at native state stabilization. Estimated $\Delta G_{\text{fold}} \sim 5\text{--}15$ kcal/mol $\approx (3.5 \times 10^{-20}\text{--}1.0 \times 10^{-19})$ J, consistent with collapsing $D_{\text{eff}} \sim 20\text{--}50$ effective dimensions.

C.2 Neural Population as Camera-Engine

Consider a neural population making a perceptual decision. The substrate is formally infinite-dimensional (continuous electromagnetic fields, cross-frequency phase coupling, continuous membrane voltage), but at typical recording resolutions (1ms, $100\mu\text{V}$ sensitivity), only $D_{\text{eff}} \sim 100$ is thermodynamically accessible.

Camera phase (0–100 ms): Environmental photon arrivals at $\sim 10^6$ rods/cones.

Each photon at 500–600 nm has $E \sim (3.3\text{--}4.0) \times 10^{-19} \text{ J}$ ($\sim 80\text{--}96 k_{\text{B}}T$), but timing is sub-Landauer. Accessible modes $D_{\text{eff}} \sim 100$ integrate timing patterns. Internal voltage landscape becomes isomorphic to environmental light pattern through weak coupling. No bits written—structural correlation emerges.

Engine phase (concurrent): Attention modulates sensory gain via weak top-down connections. Each feedback synapse $\sim 10^{-22} \text{ J} \ll k_{\text{B}}T \ln 2$, but $D_{\text{eff}} \sim 100$ feedback channels coordinately bias processing. Environment steered toward task-relevant features using internal map built during camera phase.

Collapse (at decision, $\sim 150 \text{ ms}$): Motor output: "left" vs "right" (binary). Dimensional collapse: accessible slice $D_{\text{eff}} \sim 100 \rightarrow D' = 1$. Dissipation: $\sim 100k_{\text{B}}T \ln 2 \approx 3 \times 10^{-19} \text{ J}$. Digital would pay this during every timestep; biological pays once at decision.

C.3 Cross-Scale Pattern

Table 3: Path degeneracy across biological scales

System	Event energy	D_{eff}	Estimated $\log_{10} \Omega$
Protein folding	$1\text{--}10k_{\text{B}}T$	20–50	42–94
Ca^{2+} waves	$5\text{--}20k_{\text{B}}T$	30–100	25–40
Gene regulation	$5\text{--}15k_{\text{B}}T$	10–30	15–20
Neural (ephaptic)	$\sim 10^{-3}k_{\text{B}}T \ln 2$	50–200	50–100

Common mechanism: Thermal noise explores vast micro-trajectory spaces; weak fields bias ensembles; thermodynamic cost concentrates at collapse to discrete outputs.

D Appendix C: Estimating D_{eff} and κ from Data

Data and preprocessing. Acquire $X \in \mathbb{R}^{T \times M}$ (time \times channels). Band-limit to the frequency band of interest with zero-phase FIR; extract analytic signal $z_m(t)$ via Hilbert transform for phase-based measures.

Feature matrix. Either (i) use covariance $C = \frac{1}{T-1}(X - \bar{X})^\top(X - \bar{X})$, or (ii) build a phase-coherence matrix W with entries $W_{ij} = \left| \frac{1}{T} \sum_t e^{i(\phi_i(t) - \phi_j(t))} \right|$ (inter-site phase coherence, ISPC [10]). Normalize W to unit trace to avoid scale artifacts.

Eigen-spectrum and participation ratio. Let $\{\lambda_k\}$ be eigenvalues of C (or W), sorted descending. Define

$$D_{\text{eff}} = \frac{(\sum_k \lambda_k)^2}{\sum_k \lambda_k^2}.$$

Report $D_{\text{eff}}(t)$ in a sliding window (e.g., 200 ms with 10 ms hop) to track task-locked changes.

Correlation factor κ . Construct S surrogate datasets that preserve marginal power spectra while destroying inter-channel timing dependencies. **Important:** A constant phase offset ($z_m(t) \mapsto e^{i\theta_m} z_m(t)$) does *not* break phase-coherence measures like ISPC, since $|\phi_i - \phi_j|$ is invariant to constant offsets. Instead, use one of:

- **Circular time-shift:** shift each channel by a random lag τ_m : $z_m(t) \mapsto z_m(t + \tau_m \bmod T)$;
- **Fourier phase randomization:** replace frequency-domain phases with independent uniform random phases per channel while preserving amplitude spectrum;
- **Block shuffle:** divide each channel into blocks and shuffle block order independently across channels.

Compute $D_{\text{eff}}^{(\text{sur})}$ on each surrogate; define

$$\kappa \equiv \frac{D_{\text{eff}}^{\text{sur}}}{D_{\text{eff}}^{\text{data}}} \quad (\kappa \geq 1).$$

Note: surrogates typically have *higher* D_{eff} (less coordinated structure), so $\kappa = D_{\text{eff}}^{\text{sur}}/D_{\text{eff}}^{\text{data}}$ captures how much correlation constrains dimensionality. Use κ in Ω -scaling as in Eq. 1.3.

Robustness notes. (1) Z-score channels before C to prevent amplitude-dominated modes. (2) Repeat analyses across bands (theta/alpha/beta), aligning with task epochs. (3) Control for sample size by fixing window length and applying Ledoit–Wolf shrinkage on C if M is large relative to T .